We are IntechOpen, the world's leading publisher of Open Access books Built by scientists, for scientists

6,900
Open access books available

186,000
International authors and editors

200M
Downloads

Our authors are among the

154
Countries delivered to

TOP 1%
most cited scientists

12.2%
Contributors from top 500 universities

BOOK CITATION INDEX
CLARIVATE ANALYTICS
INDEXED

WEB OF SCIENCE™

Selection of our books indexed in the Book Citation Index
in Web of Science™ Core Collection (BKCI)

Interested in publishing with us?
Contact book.department@intechopen.com

Numbers displayed above are based on latest data collected.
For more information visit www.intechopen.com

First-Principles Study of ABO_3: Role of the B–O Coulomb Repulsions for Ferroelectricity and Piezoelectricity

Kaoru Miura

Corporate R&D Headquarters, Canon Inc., Shimomaruko, Ohta, Tokyo
Japan

1. Introduction

Since Cohen (Cohen & Krakauer, 1990; Cohen, 1992) proposed an origin for ferroelectricity in perovskite oxides, investigations of ferroelectric materials using first-principles calculations have been extensively studied (Ahart et al., 2008; Bévillon et al., 2007; Bousquet et al., 2006; Chen et al., 2004; Diéguez et al., 2005; Furuta & Miura, 2010; Khenata et al., 2005; Kornev et al., 2005; Miura & Tanaka, 1998; Miura, 2002; Miura et al., 2009; 2010a;b; Miura & Furuta, 2010; Miura et al., 2011; Oguchi et al., 2009; Ricinschi et al., 2006; Uratani et al., 2008; Vanderbilt, 2000; Z. Wu et al., 2005). Currently, using the pseudopotential (PP) methods, most of the crystal structures in ferroelectric perovskite oxides (ABO_3) as well as perovskite-related oxides can be precisely predicted. However, it is also known that the most stable structures of ABO_3 optimized by the first-principles PP methods are sometimes inconsistent with the experimental results.

BaTiO$_3$ is a well-known ferroelectric ABO_3, and shows the tetragonal structure at room temperature. However, even in this well-known material, the optimized structure by the PP methods of first-principles calculations is strongly dependent on the choice of the Ti PPs, i.e., preparation for Ti 3s and 3p semicore states in addition to Ti 3d and 4s valence states is essential to the appearance of the tetragonal structure. This is an important problem for ferroelectricity, but it has been generally recognized for a long time that this problem is within an empirical framework of the calculational technics (Gonze et al., 2005).

It is known that ferroelectric state appears when the long-range forces due to the dipole-dipole interaction overcome the short-range forces due to the Coulomb repulsions. Cohen (Cohen & Krakauer, 1990; Cohen, 1992) proposed that the hybridization between Ti 3d state and O 2p state (Ti 3d–O 2p) in BaTiO$_3$ and PbTiO$_3$, which weakens the short-range force of the Coulomb repulsions between Ti and O ions, is origin of ferroelectricity. However, it seems to be difficult to consider explicitly whether the long-range force due to the dipole-dipole interaction can or cannot overcome the short-range force only with the Ti 3d–O 2p hybridization. Investigations about the relationship between the Ti–O Coulomb repulsions and the appearance of ferroelectricity were separately reported. Theoretically, we previouly investigated (Miura & Tanaka, 1998) the influence of the Ti–O$_z$ Coulomb repulsions on Ti ion displacement in tetragonal BaTiO$_3$ and PbTiO$_3$, where O$_z$ denotes the O atom to the z-axis (Ti is displaced to the z-axis). Whereas the hybridization between Ti 3d state and O$_z$ 2p$_z$ state stabilize Ti ion displacement, the strong Coulomb repulsions between Ti 3s and 3p$_z$

states and O $2p_z$ states do not favourably cause Ti ion displacement. Experimentally, on the other hand, Kuroiwa *et al.* (Kuroiwa et al., 2001) showed that the appearance of ferroelectric state is closely related to the total charge density of Ti–O bondings in BaTiO$_3$. As discussed above, investigation about a role of Ti 3s and 3p states is important in the appearance of the ferroelectric state in tetragonal BaTiO$_3$.

It has been generally known (Miura & Furuta, 2010) that the most stable structure of ABO_3 is closely related to the tolerance factor t,

$$t \equiv \frac{r_A + r_O}{\sqrt{2}\,(r_B + r_O)} \quad , \tag{1}$$

where r_A, r_B, and r_O denote the ionic radii of A, B, and O ions, respectively. Generally, the most stable structure is tetragonal for $t \gtrsim 1$, cubic for $t \approx 1$, and rhombohedral or orthorhombic for $t \lesssim 1$. In fact, BaTiO$_3$ ($t = 1.062$) and SrTiO$_3$ ($t = 1.002$) show tetragonal and cubic structures in room temperature, respectively. However, under external pressure, e.g., hydrostatic or in-plane pressure (Ahart et al., 2008; Fujii et al., 1987; Haeni et al., 2004), the most stable structures of ABO_3 generally change; e.g., SrTiO$_3$ shows the tetragonal and ferroelectric structure even in room temperature when the a lattice parameter along the [100] axis (and also the [010] axis) is smaller than the bulk lattice parameter with compressive stress (Haeni et al., 2004). Theoretical investigations of ferroelectric ABO_3 under hydrostatic or in-plane pressure by first-principles calculations have been reported (Bévillon et al., 2007; Diéguez et al., 2005; Furuta & Miura, 2010; Khenata et al., 2005; Kornev et al., 2005; Miura et al., 2010a; Ricinschi et al., 2006; Uratani et al., 2008; Z. Wu et al., 2005), and their calculated results are consistent with the experimental results. However, even in BaTiO$_3$, which are a well-known lead-free ferroelectric and piezoelectric ABO_3, few theoretical papers about the piezoelectric properties with in-plane compressive stress have been reported.

Recently, we investigated the roles of the Ti–O Coulombrepulsions in the appearance of a ferroelectric states in tetragonal BaTiO$_3$ by the analysis of a first-principles PP method (Miura et al., 2010a). We investigated the structural properties of tetragonal and rhombohedral BaTiO$_3$ with two kind of Ti PPs, and propose the role of Ti 3s and 3p states for ferroelectricity. Moreover, we also investigated the structural, ferroelectric, and piezoelectric properties of tetragonal BaTiO$_3$ and SrTiO$_3$ with in-plane compressive structures (Furuta & Miura, 2010). We discussed the difference in the piezoelectric mechanisms between BaTiO$_3$ and SrTiO$_3$ with in-plane compressive structures, which would be important for piezoelectric material design. In this chapter, based on our previous reports (Furuta & Miura, 2010; Miura et al., 2010a), the author discusses a general role of B–O Coulomb repulsions for ferroelectricity and piezoelectricity in ABO_3, especially in BaTiO$_3$ and SrTiO$_3$.

2. Calculations

Calculations of BaTiO$_3$ and SrTiO$_3$ were performed using the ABINIT package code (Gonze et al., 2002), which is one of the norm-conserving PP (NCPP) methods. Electron-electron interaction was treated in the local-density approximation (LDA) (Perdew & Wang, 1992). Pseudopotentials were generated using the OPIUM code (Rappe, 2004):

(i) In order to investigate the role of Ti 3s and 3p states for BaTiO$_3$, two kinds of Ti PPs were prepared: one is the Ti PP with 3s, 3p, 3d and 4s electrons treated as semicore or valence electrons (Ti3spd4s PP), and the other is the Ti PP with only 3d and 4s electrons treated as valence electrons (Ti3d4s PP). The above seudopotentials were generated using the OPIUM

code (Rappe, 2004), and the differences between the calculated result and the experimental one are within 1.5 % of the lattice parameter and within 10 % of the bulk modulus in the optimized calculation of bulk Ti in both PPs. Moreover, Ba PP with 5s, 5p and 6s electrons treated as semicore or valence electrons, and O PP with 2s and 2p electrons treated as semicore or valence electrons, were also prepared. The cutoff energy for plane-wave basis functions was set to be 50 Hartree (Hr). A $6\times6\times6$ Monkhorst-Pack k-point mesh was set in the Brillouin zone of the unit cell. The number of atoms in the unit cell was set to be five, and positions of all the atoms were optimized within the framework of the tetragonal ($P4mm$) or rhombohedral ($R3m$) structure.

(ii) The ferroelectric and piezoelectric properties of SrTiO$_3$ and BaTiO$_3$ with compressive tetragonal structures are investigated. Pseudopotentials were generated using the OPIUM code (Rappe, 2004); 4s (5s), 4p (5p) and 5s (6s) electrons for Sr (Ba), 3s, 3p, 3d and 4s electrons for Ti, and 2s and 2p electrons for O were treated as semicore or valence electrons. The cutoff energy fo the plane wave basis functions was set to be 50 Hr. A $6\times6\times6$ Monkhorst-Pack k-point mesh was set in the Brillouin zone of the unit cell. The number of atoms in the ABO_3 unit cell was set to be five, and the coordinations of all the atoms were optimized within a framework of the tetragonal ($P4mm$) structure. An $6 \times 6 \times 6$ Monkhorst-Pack k-point sampling was set in Brillouin zone of the unit cell.

In the present calculations, spontaneous polarizations and piezoelectric constants were also evaluated, due to the Born effective charges (Resta, 1994) and density-functional perturbation theory (Hamann et al., 2005; X. Wu et al., 2005). The spontaneous polarization of tetragonal structures along the [001] axis, P_3, is defined as,

$$P_3 \equiv \sum_k \frac{ec}{\Omega} Z_{33}^*(k) u_3(k) , \qquad (2)$$

where e, c, and Ω denote the charge unit, the lattice parameter of the unit cell along the [001] axis, and the volume of the unit cell, respectively. $u_3(k)$ denotes the displacement along the [001] axis of the kth atom, and $Z_{33}^*(k)$ denotes the Born effective charges (Resta, 1994) which contributes to the P_3 from the $u_3(k)$. The piezoelectric e constants, on the other hand, are defined as

$$e_{\alpha\beta} \equiv \left(\frac{\partial P_\alpha}{\partial \eta_\beta} \right)_u + \sum_k \left(\frac{\partial P_\alpha}{\partial u_\alpha(k)} \right)_\eta \frac{\partial u_\alpha(k)}{\partial \eta_\beta} , \qquad (3)$$

where P, η, and $u(k)$ denote the spontaneous polarization, the strain, and the displacement of the kth atom, respectively. α and β denote the direction-indexes of the axis, i.e., 1 along the [100] axis, 2 along the [010] axis, and 3 along the [001] axis, respectively. In eq. (3), the first term of the right hand denotes the clamped term evaluated at vanishing internal strain, and the second term denotes the relaxed term that is due to the relative displacements. According to the eqs. (2) and (3), therefore, e_{33} or e_{31} can be especially written as,

$$e_{3\beta} = \left(\frac{\partial P_3}{\partial \eta_\beta} \right)_u + \sum_k \frac{ec}{\Omega} Z_{33}^*(k) \frac{\partial u_3(k)}{\partial \eta_\beta} \qquad (\beta = 3,1) . \qquad (4)$$

(a) P4mm $BaTiO_3$: c/a v.s. a

(b) P4mm $BaTiO_3$: δ_{Ti} v.s. a
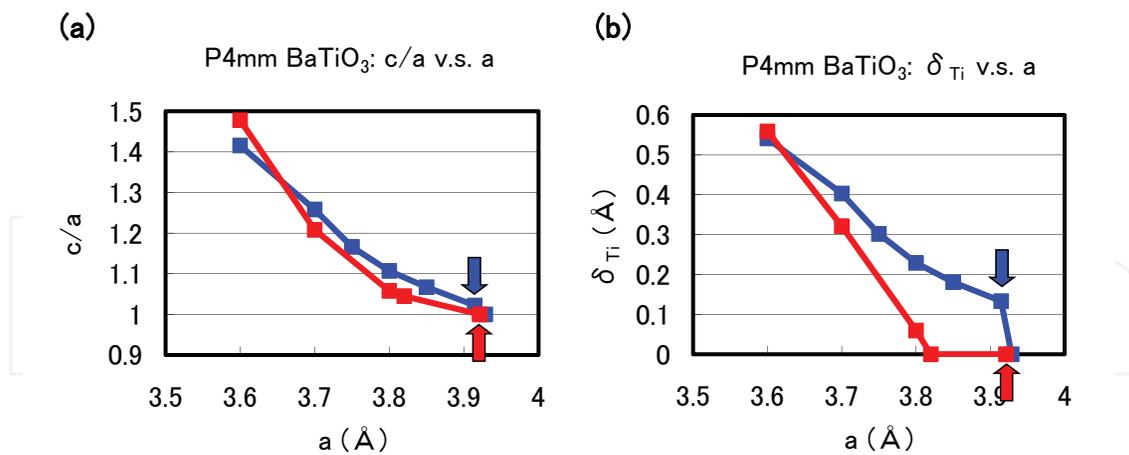
Fig. 1. Optimized calculated results as a function of a lattice parameters in tetragonal $BaTiO_3$: (a) c/a ratio and (b) δ_{Ti} to the [001] axis. Blue lines correspond to the results with the Ti3spd4s PP, and red lines correspond to those with the Ti3d4s PP. Results with arrows are the fully optimized results, and the other results are those with c and all the inner coordinations optimized for fixed a (Miura et al., 2010a).


P4mm $BaTiO_3$: Density of States
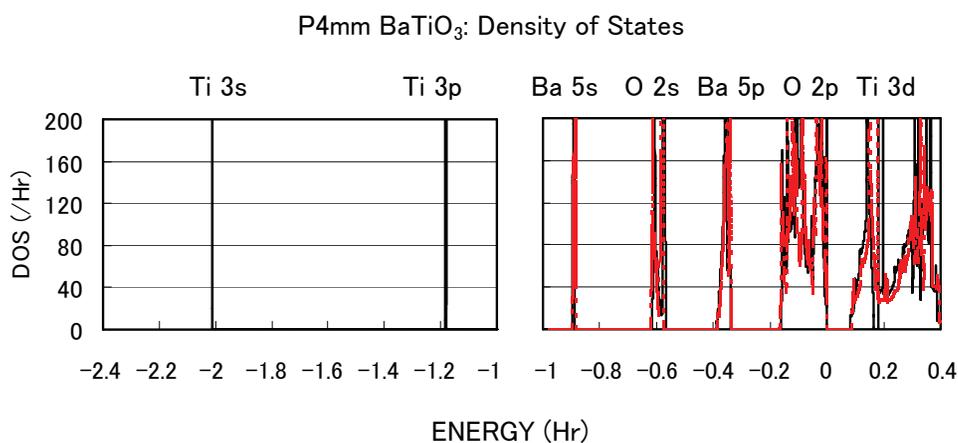
Fig. 2. Total density of states (DOS) of fully optimized tetragonal $BaTiO_3$ with the Ti3spd4s PP (solid line) and cubic $BaTiO_3$ with the Ti3d4s PP (red dashed line) (Miura et al., 2010a).

3. Results and discussion

3.1 $BaTiO_3$: Role of Ti 3s and 3p states for ferroelectricity

In this subsection, the author discusses the role of Ti 3s and 3p states for ferroelectricity for ferroelectricity in tetragonal $BaTiO_3$.

Figures 1(a) and 1(b) show the optimized results for the ratio c/a of the lattice parameters and the value of the Ti ion displacement (δ_{Ti}) as a function of the a lattice parameters in tetragonal $BaTiO_3$, respectively. Results with arrows are the fully optimized results, and the others results are those with the c lattice parameters and all the inner coordinations optimized for fixed

a. Note that the fully optimized sturucture of BaTiO$_3$ is tetragonal with the Ti3spd4s PP, whereas it is cubic ($Pm\bar{3}m$) with the Ti3d4s PP. As shown in Fig. 1(a) and 1(b), c/a and δ_{Ti} show significantly different results for $a \gtrsim 3.7$ whereas they show almost the same results for $a \lesssim 3.7$, for both Ti PPs. This result suggests that the optimized results of ABO_3 with smaller lattice parameters, e.g., under high pressure (Bévillon et al., 2007), are almost independent of the choice of PP.
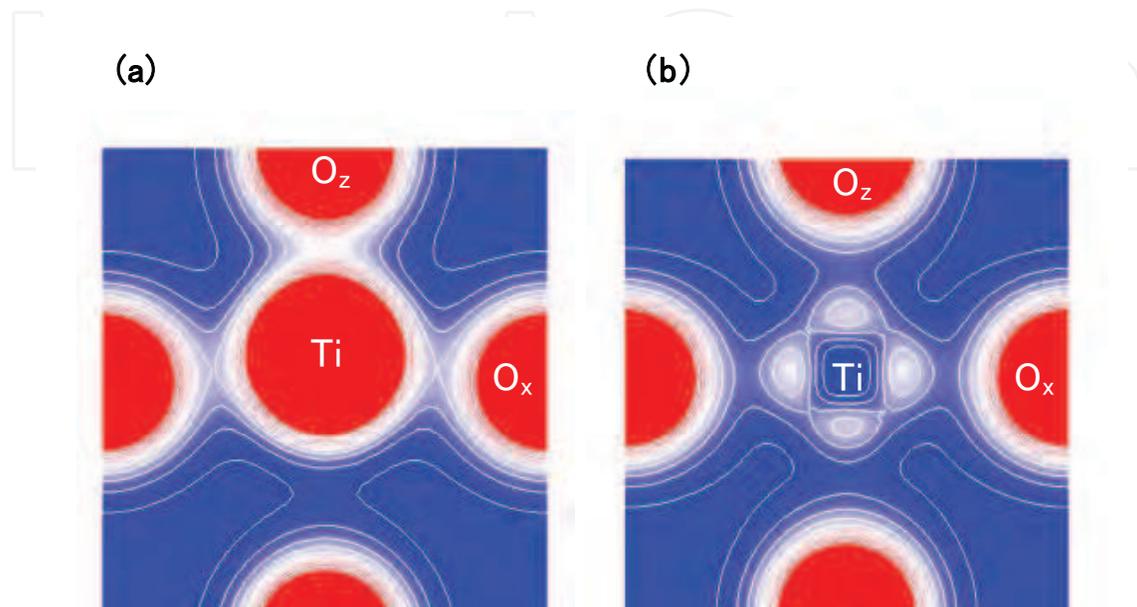
Fig. 3. Two-dimentional electron-density contour map on the xz-plane for tetragonal BaTiO$_3$: (a) with the Ti3spd4s PP, and (b) with the Ti3d4s PP. The optimized calculated results with a fixed to be 3.8 are shown in both figures. The electron density increases as color changes from blue to red via white. Contour curves are drawn from 0.4 to 2.0 $e/^3$ with increments of 0.2 $e/^3$ (Miura et al., 2010a).

The calculated results shown in Fig. 1 suggest that the explicit treatment of Ti 3s and 3p semicore states is essential to the appearance of ferroelectric states in BaTiO$_3$. In the following, the author investigates the role of Ti 3s and 3p states for ferroelectricity from two viewpoints. One viwpoint concerns hybridizations between Ti 3s and 3p states and other states. Figure 2 shows the total density of states (DOS) of tetragonal BaTiO$_3$ with two Ti PPs. Both results are in good agreement with previous calculated results (Chen et al., 2004; Khenata et al., 2005) by the full-potential linear augmented plane wave (FLAPW) method. In the DOS with the Ti3spd4s PP, the energy "levels", not bands, of Ti 3s and 3p states, are located at -2.0 Hr and -1.2 Hr, respectively. This result suggests that the Ti 3s and 3p orbitals do not make any hybridizations but only give Coulomb repulsions with the O orbitals as well as the Ba orbitals. In the DOS with the Ti3d4s PP, on the other hand, the energy levels of Ti 3s and 3p states are not shown because Ti 3s and 3p states were treated as the core charges. This result means that the Ti 3s and 3p orbitals cannot even give Coulomb repulsions with the O orbitals as well as the Ba orbitals.

Another viewpoint is about the Coulomb repulsions between Ti 3s and 3p$_{x(y)}$ states and O$_{x(y)}$ 2s and 2p$_{x(y)}$ states in tetragonal BaTiO$_3$. Figures 3(a) and 3(b) show two-dimentional electron-density contour map on the xz-plane for tetragonal BaTiO$_3$ with the Ti3spd4s PP, and that with the Ti3d4s PP, respectively. These are the optimized calculated results with a fixed
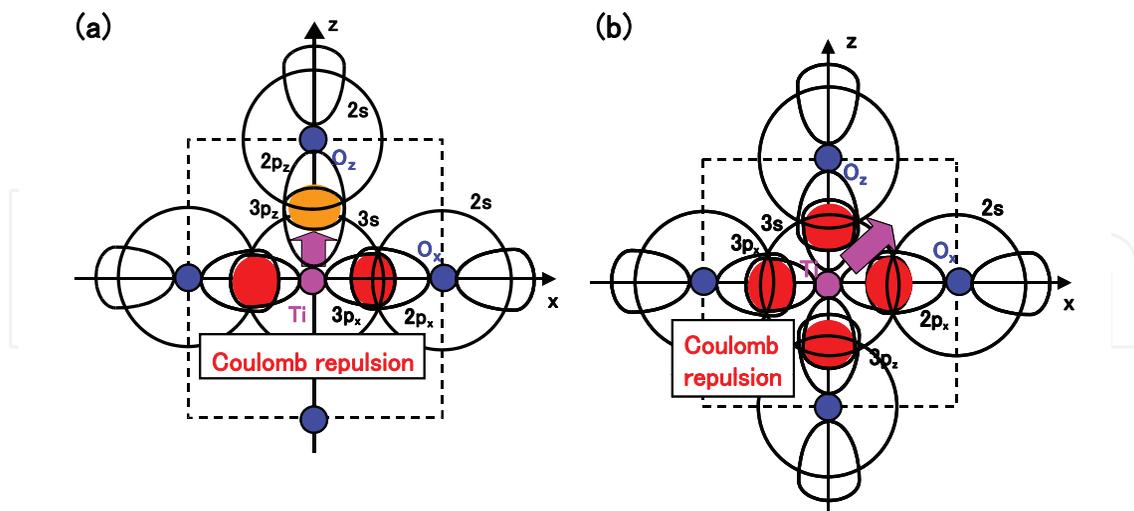
Fig. 4. Illustrations of the proposed mechanisms for the Coulomb repulsions between Ti 3s and 3p states and O 2s and 2p states in BaTiO$_3$: (a) anisotropic Coulomb repulsions between Ti 3s and 3p$_{x\,(y)}$ states and O$_{x\,(y)}$ 2s and 2p$_{x\,(y)}$ states, and between Ti 3s and 3p$_z$ states and O$_z$ 2s and 2p$_z$ states, in the tetragonal structure. (b) isotropic Coulomb repulsions between Ti 3s and 3p$_{x\,(y)\,(z)}$ states and O$_{x\,(y)\,(z)}$ 2s and 2p$_{x\,(y)\,(z)}$ states, in the rhombohedral structure (Miura et al., 2010a).

to be 3.8 , and the electron density in Fig. 3(a) is quantitatively in good agreement with the experimental result (Kuroiwa et al., 2001). The electron density between Ti and O$_x$ ions in Fig. 3(a) is larger than that in Fig. 3(b), which suggests that Ti ion displacement is closely related to the Coulomb repulsions between Ti 3s and 3p states and O 2s and 2p states along the [001] axis (the z-axis in this case).

The present discussion of the Coulomb repulsions is consistent with the previous reports. A recent soft mode investigation (Oguchi et al., 2009) of BaTiO$_3$ shows that Ba ions contribute little to the appearance of Ti ion displacement along the [001] axis. This result suggests that Ti ion displacement is closely related to the structural distortion of TiO$_6$ octahedra. In the present calculations, on the other hand, the only difference between BaTiO$_3$ with the Ti3spd4s PP and with the Ti3d4s PP is the difference in the expression for the Ti 3s and 3p states, i.e., the explicit treatment and including core charges. However, our previous calculation (Miura & Tanaka, 1998) shows that the strong Coulomb repulsions between Ti 3s and 3p$_z$ states and O$_z$ 2s and 2p$_z$ states do not favour Ti ion displacement along the [001] axis. This result suggests that the Coulomb repulsions between Ti 3s and 3p$_{x\,(y)}$ states and O$_{x\,(y)}$ 2s and 2p$_{x\,(y)}$ states would contribute to Ti ion displacement along the [001] axis, and the suggestion is consistent with a recent calculation (Uratani et al., 2008) for PbTiO$_3$ indicating that the tetragonal and ferroelectric structure appears more favourable as the *a* lattice parameter decreases.

Considering the above investigations, the author proposes the mechanism of Ti ion displacement as follows: Ti ion displacement along the z-axis appears when the Coulomb repulsions between Ti 3s and 3p$_{x\,(y)}$ states and O$_{x\,(y)}$ 2s and 2p$_{x\,(y)}$ states, in addition to the dipole-dipole interaction, overcome the Coulomb repulsions between Ti 3s and 3p$_z$ states and O$_z$ 2s and 2p$_z$ states (Miura & Tanaka, 1998). An illustration of the Coulomb repulsions is shown in Fig. 4(a). In fully optimized BaTiO$_3$ with the Ti3spd4s PP, the Ti ion can be displaced due to the above mechanism. In fully optimized BaTiO$_3$ with the Ti3d4s PP, on the other

hand, the Ti ion cannot be displaced due to the weaker Coulomb repulsions between Ti and O$_{x(y)}$ ions. However, since the Coulomb repulsion between Ti and O$_z$ ions in BaTiO$_3$ with the Ti3d4s PP is also weaker than that in BaTiO$_3$ with the Ti3spd4s PP, the Coulomb repulsions between between Ti and O$_{x(y)}$ ions in addition to the log-range force become comparable to the Coulomb repulsions between Ti and O$_z$ ions both in Ti PPs, as the lattice parameter a becomes smaller. The above discussion suggests that the hybridization between Ti 3d and O$_z$ 2s and 2p$_z$ stabilizes Ti ion displacement, but contribute little to a driving force for the appearance of Ti ion displacement.

It seems that the above proposed mechanism for tetragonal BaTiO$_3$ can be applied to the mechanism of Ti ion displacement in rhombohedral BaTiO$_3$, as illustrated in Fig. 4(b). The strong isotropic Coulomb repulsions between Ti 3s and 3p$_{x(y)(z)}$ states and O$_{x(y)(z)}$ 2s and 2p$_{x(y)(z)}$ states yield Ti ion displacement along the [111] axis. On the other hand, when the isotropic Coulomb repulsions are weaker or stronger, the Ti ion cannot be displaced and therefore it is favoured for the crystal structure to be cubic.

(a)   (b)
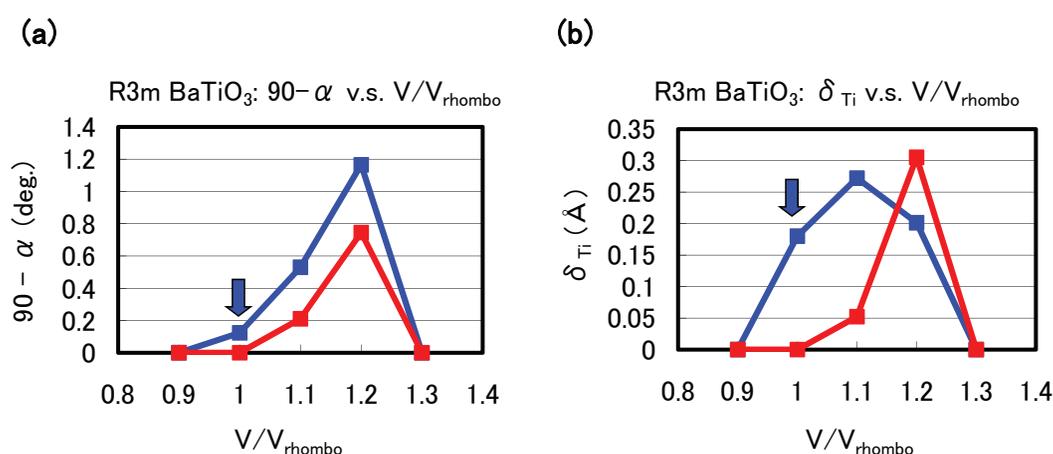
Fig. 5. Optimized calculated results as a function of the fixed volumes of the unit cells in rhombohedral BaTiO$_3$: (a) 90$-\alpha$ degree and (b) δ_{Ti} to the [111] axis. Blue lines correspond to the results with the Ti3spd4s PP, and red lines correspond to those with the Ti3d4s PP. V_{rhombo} denote the volume of the fully optimized unit cell with the Ti 3spd4s PP. Results with arrows are the fully optimized results, and the other results are those with all the inner coordinations optimized for fixed volumes of the unit cells (Miura et al., 2010a).

Let us investigate the structural properties of rhombohedral BaTiO$_3$. Figures 5(a) and 5(b) show the optimized results of the 90$-\alpha$ degree and δ_{Ti} as a function of fixed volumes of the unit cells in rhombohedral BaTiO$_3$, respectively, where α denotes the angle between two lattice vectors. In these figures, α denotes the angle between two crystal axes of rhombohedral BaTiO$_3$, and δ_{Ti} denotes the value of the Ti ion displacement along the [111] axis. Results with arrows are the fully optimized results; V_{rhombo} denote the volume of the fully optimized unit cell with the Ti 3spd4s PP. The other results are those with all the inner coordinations optimized with fixed volumes of the unit cells. The proposal mechanisms about the Coulomb repulsions seem to be consistent with the calculated results shown in Fig. 5: For $V/V_{rhombo} \lesssim 0.9$ or $\gtrsim 1.3$, the isotropic Coulomb repulsions are weaker or stronger, and the Ti ion cannot be displaced along the [111] axis and therefore the crystal structure is cubic for both Ti PPs. For $0.9 \lesssim V/V_{rhombo} \lesssim 1.3$, on the other hand, the isotropic Coulomb repulsions

are strong enough to yield Ti ion displacement for both Ti PPs. However, since the magnitude of the isotropic Coulomb repulsion is different in the two Ti PPs, the properties of the $90-\alpha$ degree and δ_{Ti} are different quantitatively.

3.2 Role of the Ti–O Coulomb repulsions for piezoelectric SrTiO$_3$ and BaTiO$_3$

As discussed in the previous subsection, the Coulomb repulsions between Ti 3s and $3p_{x(y)}$ states and $O_{x(y)}$ 2s and $2p_{x(y)}$ states have an important role in the appearance of the ferroelectric state in tetragonal BaTiO$_3$. In this subsection, the author discusses the role of the Ti–O Coulomb repulsions for piezoelectric SrTiO$_3$ and BaTiO$_3$.
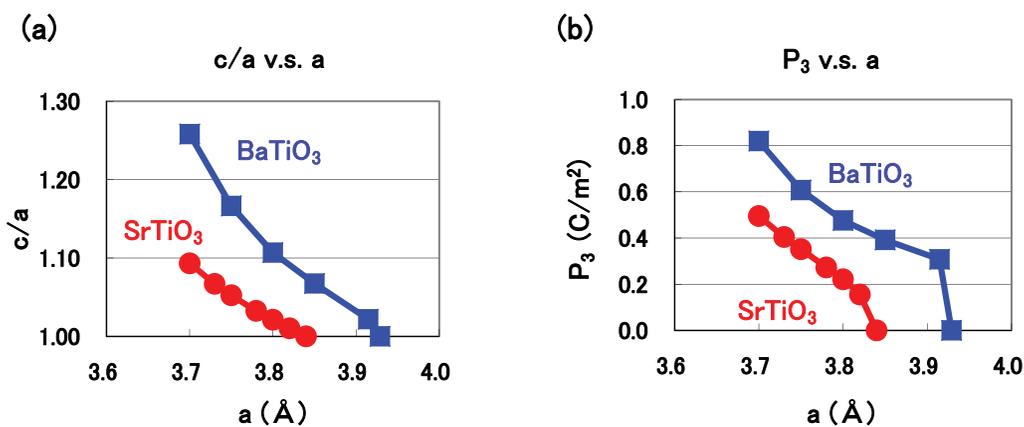
Fig. 6. Optimized calculated results as a function of a lattice parameters in compressive tetragonal SrTiO$_3$ and BaTiO$_3$: (a) c/a ratio and (b) P_3, i.e., spontaneous polarization along the [001] axis (Furuta & Miura, 2010).
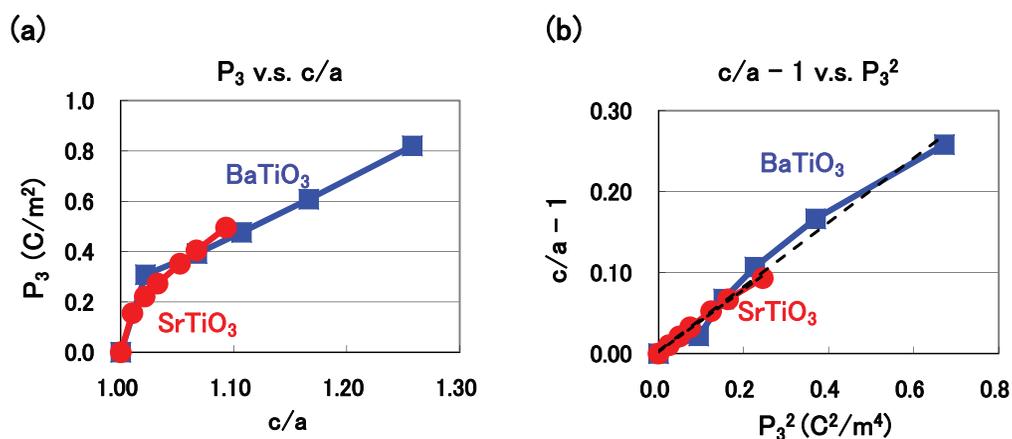
Fig. 7. (a) P_3 as a function of c/a ratios, and (b) c/a ratio as a function of P_3^2. These values are derived from the calculated results as shown in Figs. 6(a) and (b). Dotted and dashed lines in Fig. 7(b) serve as visual guides for SrTiO$_3$ and BaTiO$_3$, respectively (Furuta & Miura, 2010).

Figures 6(a) shows the optimized results for the ratio c/a as a function of the a lattice parameters in tetragonal SrTiO$_3$ and BaTiO$_3$. These results are the fully optimized results and the results with the c lattice parameters and all the inner coordinations optimized for

fixed a. The fully optimized parameters of SrTiO$_3$ (a = 3.84 : cubic) and BaTiO$_3$ (a = 3.91 and c = 4.00 : tetragonal) are within 2.0% in agreement with the experimental results in room temperature. Figures 6(b) shows the evaluated results for P_3 as a function of the a lattice parameters in tetragonal SrTiO$_3$ and BaTiO$_3$, where P_3, which is evaluated by eq. (2), denotes the spontaneous polarization along the [001] axis. Note that the tetragonal and ferroelectric structures appear even in SrTiO$_3$ when the fixed a lattice parameter is compressed to be smaller than the fully-optimized a lattice parameter. As shown in Figs. 6(a) and 6(b), the tetragonal and ferroelectric structure appear more favorable as the fixed a lattice parameter decreases, which is consistent with previous calculated results (Miura et al., 2010a; Ricinschi et al., 2006; Uratani et al., 2008). The results would be due to the suggestion discussed in the previous section that the large Coulomb repulsion of Ti–O bondings along the [100] axis (and the [010] axis) is a driving force of the displacement of Ti ions along the [001] axis, i.e., the large Coulomb repulsion along the [100] axis (and the [010] axis) is essential for the appearance of the tetragonal structure. Figure 7(a) shows the relationship between P_3 and the ratio c/a, where P_3 and c/a are derived from the calculated results shown in Figs. 6(a) and 6(b). The property of BaTiO$_3$ in Fig. 7(a) is in qualitatively agreement with a previous calculational result (Ricinschi et al., 2006). Figure 7(b) shows the relationship between the ratio c/a and P_3^2. Note that $c/a - 1$ is proportional to P_3^2 with alomost the same coefficients in both SrTiO$_3$ and BaTiO$_3$. Clearly, the ratio c/a is a good parameter in both tetragonal SrTiO$_3$ and BaTiO$_3$ with in-plane compressive stress. Therefore, in the following, the author uses the ratio c/a as a parameter for the investigations of the piezoelectric properties.
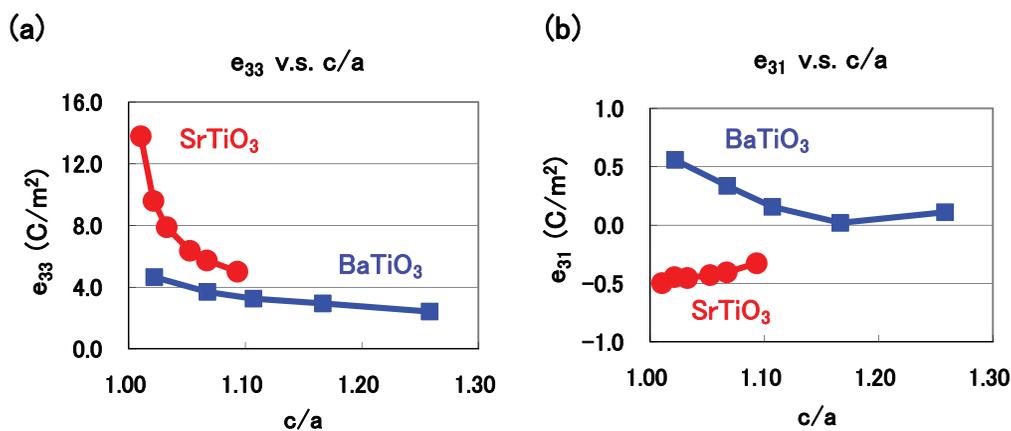

Fig. 8. Evaluated piezoelectric constants as a function of c/a ratios in optimized tetragonal SrTiO$_3$ and BaTiO$_3$: (a) e_{33} and (b) e_{31} (Furuta & Miura, 2010).

Figures 8(a) and 8(b) shows the piezoelectric properties of e_{33} and e_{31} as a function of the ratio c/a in tetragonal SrTiO$_3$ and BaTiO$_3$. The ratio c/a is optimized value as shown in Fig. 6(a) and e_{33} and e_{31} are evaluated values in their optimized structures. Note that e_{33} become larger at $c/a \approx 1$, especially in SrTiO$_3$. These properties seem to be similar to the properties arond the Curie temperatures in piezoelectric ABO_3; Damjanovic emphasized the importance of the polarization extension as a mechanism of larger piezoelectric constants in a recent paper (Damjanovic, 2010). Contrary to e_{33}, on the other hand, the changes in e_{31} are much smaller than the changes in e_{33}, but note that e_{31} shows negative in SrTiO$_3$ while positive in BaTiO$_3$.
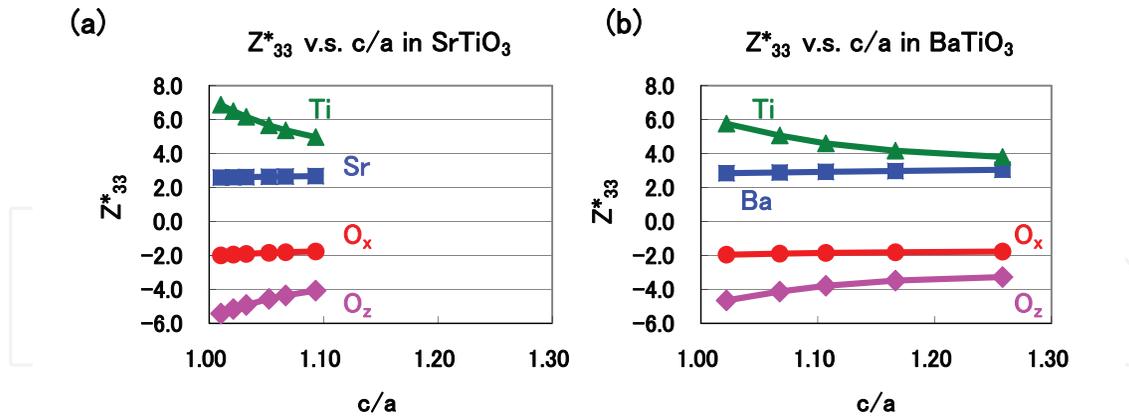
Fig. 9. Evaluated Born effective charges $Z_{33}^*(k)$ as a function of c/a ratios: (a) SrTiO$_3$ and (b) BaTiO$_3$. O$_x$ and O$_z$ denote oxygen atoms along the [100] axis and the [001] axis, respectively (Furuta & Miura, 2010).
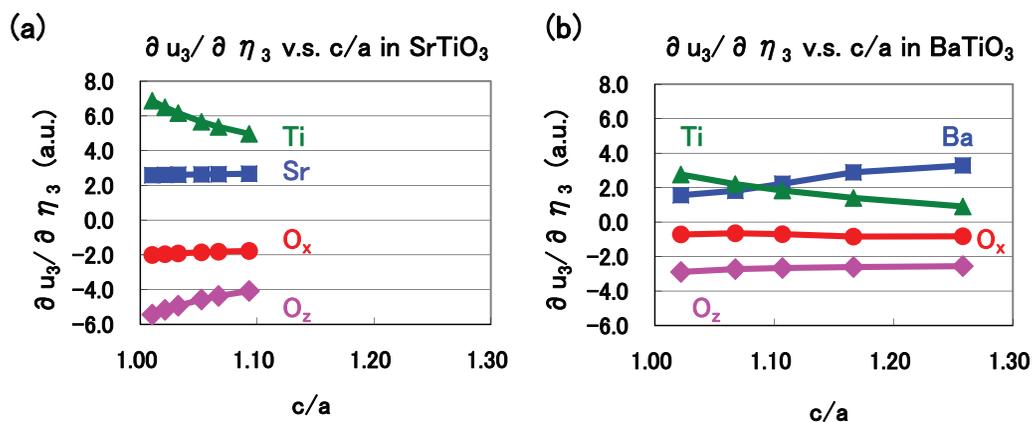

Fig. 10. Evaluated values of $\partial u_3(k)/\partial \eta_3$ as a function of c/a ratios: (a) SrTiO$_3$ and (b) BaTiO$_3$. "a.u." denotes the atomic unit (≈ 0.53) (Furuta & Miura, 2010).

As expressed in eq. (4), e_{3j} is the sum of the contributions from the clamped term and the relaxed term. However, it has been generally known that the contribution to e_{3j} from the clamped term is much smaller than that from the relaxed term; in fact, the absolute values of the e_{33} clamped terms are less than 1 C/m^2 in both SrTiO$_3$ and BaTiO$_3$. The author therefore investigates the contributions to the relaxed term of e_{33} and e_{31} in detail. As expressed in eq. (4), the relaxed terms of e_{3j} are proportional to the sum of the products between the $Z_{33}^*(k)$ and $\partial u_3(k)/\partial \eta_j$ ($j = 3$ or 1) values. Let us show the evaluated results of $Z_{33}^*(k)$, $\partial u_3(k)/\partial \eta_3$, and $\partial u_3(k)/\partial \eta_1$ in the following. Figures 9(a) and 9(b) show the $Z_{33}^*(k)$ values in SrTiO$_3$ and BaTiO$_3$, respectively. Properties of the $Z_{33}^*(k)$ values are quantitatively similar in both SrTiO$_3$ and BaTiO$_3$. Therefore, the difference in the properties of e_{33} and e_{31} between SrTiO$_3$ and BaTiO$_3$ must be due to the difference in the properties of $\partial u_3(k)/\partial \eta_j$. Figures 10(a) and 10(b) show the $\partial u_3(k)/\partial \eta_3$ values in SrTiO$_3$ and BaTiO$_3$, respectively. In these figures, O$_x$ and O$_z$ denote oxygen atoms along the [100] and [001] axes, respectively, and η_3 is defined as $\eta_3 \equiv (c - c_0)/c_0$, where c_0 denotes the c lattice parameter with fully optimized structure. Clearly, the absolute values of $\partial u_3(k)/\partial \eta_3$ are different in between SrTiO$_3$ and BaTiO$_3$. On

First-Principles Study of ABO_3: Role of the
B–O Coulomb Repulsions for Ferroelectricity and Piezoelectricity
405
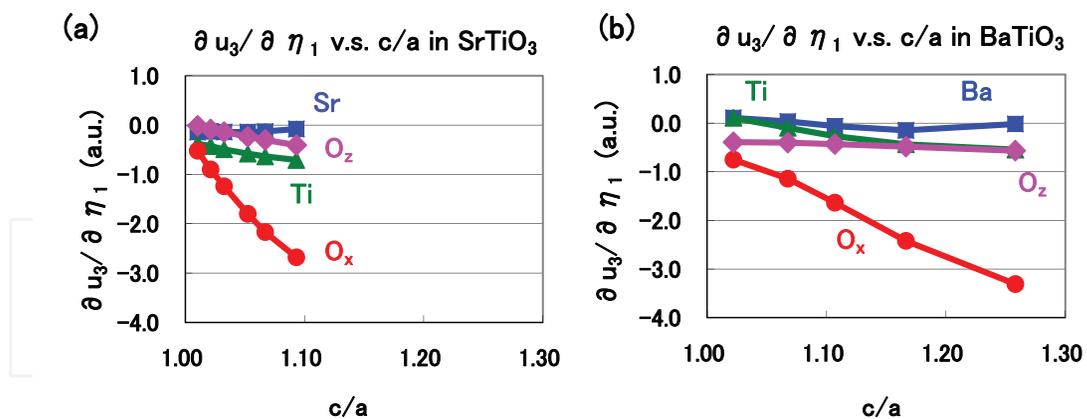
Fig. 11. Evaluated values of $\partial u_3(k)/\partial\eta_1$ as a function of c/a ratios: (a) SrTiO$_3$ and (b) BaTiO$_3$ (Furuta & Miura, 2010).

the other hand, Figs. 11(a) and 11(b) show the $\partial u_3(k)/\partial\eta_1$ values in SrTiO$_3$ and BaTiO$_3$, respectively; η_1 is defined as $\eta_1 \equiv (a - a_0)/a_0$, where a_0 denotes the a lattice parameter with fully optimized structure. The absolute values of $\partial u_3(k)/\partial\eta_1$, especially for Ti, O$_x$, and O$_z$, are different in between SrTiO$_3$ and BaTiO$_3$. As a result, the quantitative differences in e_{33} and e_{31} in between SrTiO$_3$ and BaTiO$_3$ are due to the differences in the contribution of the $\partial u_3(k)/\partial\eta_j$ values. In the following, the author would like to discuss the reasons of the quantitative differences in e_{33} and e_{31} in between SrTiO$_3$ and BaTiO$_3$.

Figure 12(a) shows the difference between the A–O$_x$ distance (R_{A-O_x}) and the sum of r_A and r_{O_x} ($r_A + r_{O_x}$) on the (100) plane as a function of the ratio c/a, where the values of the ionic radii are defined as Shannon's ones (Shannon, 1976). Note that R_{A-O_x} is smaller than $r_A + r_{O_x}$ in both SrTiO$_3$ and BaTiO$_3$. However, the difference in absolute value between R_{A-O_x} and $r_A + r_{O_x}$ in SrTiO$_3$ is much smaller than the difference in BaTiO$_3$ for $1.00 \lesssim c/a \lesssim 1.10$. This result suggests that the Sr–O$_x$ Coulomb repulsion on the (100) plane in SrTiO$_3$ is much smaller than the Ba–O$_x$ Coulomb repulsion in BaTiO$_3$ and that therefore Sr and O$_x$ ions of SrTiO$_3$ can be displaced more easily along the [001] axis than Ba and O$_x$ ions of BaTiO$_3$. This would be a reason why the absolute values of $\partial u_3(k)/\partial\eta_3$ of Sr and O$_x$ ions in SrTiO$_3$ are larger than those of Ba and O$_x$ ions in BaTiO$_3$. Figure 12(b) shows the difference between the Ti–O$_z$ distance (R_{Ti-O_z}) and $r_{Ti} + r_{O_z}$ along the [001] axis as a function of the ratio c/a. Note that R_{Ti-O_z} is smaller than $r_{Ti} + r_{O_z}$ in both SrTiO$_3$ and BaTiO$_3$. However, the difference in absolute value between R_{Ti-O_z} and $r_{Ti} + r_{O_z}$ in SrTiO$_3$ is smaller than the difference in BaTiO$_3$ for $1.00 \lesssim c/a \lesssim 1.10$. This result suggests that the Ti–O$_z$ Coulomb repulsion along the [001] axis in SrTiO$_3$ is smaller than that in BaTiO$_3$ and that therefore the Ti ion of SrTiO$_3$ can be displaced more easily along the [001] axis than that of BaTiO$_3$. This would be a reason why the absolute values of $\partial u_3(k)/\partial\eta_3$ of Ti and O$_z$ ions in SrTiO$_3$ are larger than that in BaTiO$_3$.

In the following, the author discusses the relationship between $\partial u_3(Ti)/\partial\eta_3$ and the ratio c/a in detail. Figure 13(a) shows the properties of the diffrences in the total energy (ΔE_{total}) as a function of u_{Ti}. In this figure, the properties of SrTiO$_3$ with $c/a = 1.021$ ($\eta = 0.011$), SrTiO$_3$ with $c/a = 1.093$ ($\eta = 0.053$) and BaTiO$_3$ with $c/a = 1.022$ as a reference, are shown. Calculations of E_{total} were performed with the fixed crystal structures of previously optimized structures except Ti ions. Figure 13(b) shows illustrations of ΔE_{total} curves with deviations at the minimum points of the ΔE_{total} values, corresponding to the ΔE_{total} curves of SrTiO$_3$ in Fig. 13(a). Clearly, as η_3 becomes smaller, the deviated value at the minimum point of the
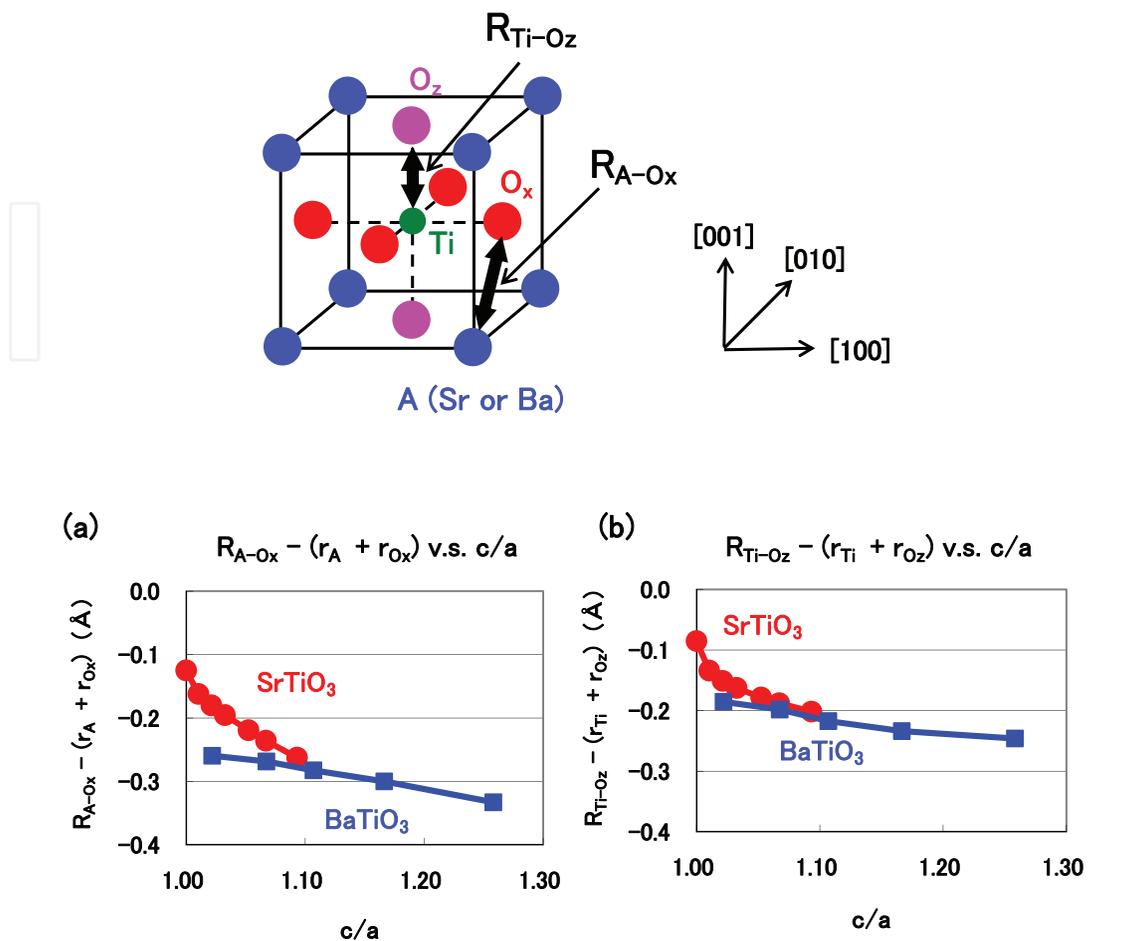
Fig. 12. Evaluated values as a function of c/a ratios in optimized tetragonal $SrTiO_3$ and $BaTiO_3$: (a) difference between the A–O_x distance (R_{A-O_x}) and $r_A + r_{O_x}$, and (b) difference between the Ti–O_z distance (R_{Ti-O_z}) and $r_{Ti} + r_{O_z}$, as a function of the ratio c/a. R_{A-O_x} and R_{Ti-O_z} in $ATiO_3$ are also illustrated; all the ionic radii are much larger, and A and Ti ions are displaced along the [001] axis in real $ATiO_3$ (Furuta & Miura, 2010).

ΔE_{total} values becomes smaller, i.e., the Ti ion can be displaced more favourably. On the other hand, as shown in Fig. 10(a), the absolute value of $\partial u_3(Ti)/\partial \eta_3$ becomes larger as η_3 becomes smaller. Therefore, the Ti ion can be displaced more favourably as the deviated value at the minimum point of the ΔE_{total} values becomes smaller.

Next, let us discuss quantitative properties of e_{31}, especially the reason why e_{31} in $SrTiO_3$ shows negative while positive in $BaTiO_3$. Figure 14(a) shows the difference between the Ti–O_x distance (R_{Ti-O_x}) and $r_{Ti} + r_{O_x}$ along the [100] axis as a function of the ratio c/a. Note that R_{Ti-O_x} is smaller than $r_{Ti} + r_{O_x}$ in both $SrTiO_3$ and $BaTiO_3$. However, the difference in absolute value between R_{Ti-O_x} and $r_{Ti} + r_{O_x}$ in $SrTiO_3$ is larger than that in $BaTiO_3$, i.e., R_{Ti-O_x} in $SrTiO_3$ is smaller than R_{Ti-O_x} in $BaTiO_3$. This result suggests that the Ti–O_x Coulomb repulsion along the [100] axis in $SrTiO_3$ is larger than that in $BaTiO_3$ and that therefore Ti and O_x ions of $SrTiO_3$ can be displaced along the [001] axis more easily than those of $BaTiO_3$, as discussed in previous subsection. This would be a reason why the absolute values of $\partial u_3(k)/\partial \eta_1$ of Ti and O_x ions in $SrTiO_3$ are larger than those in $BaTiO_3$. Therefore, each
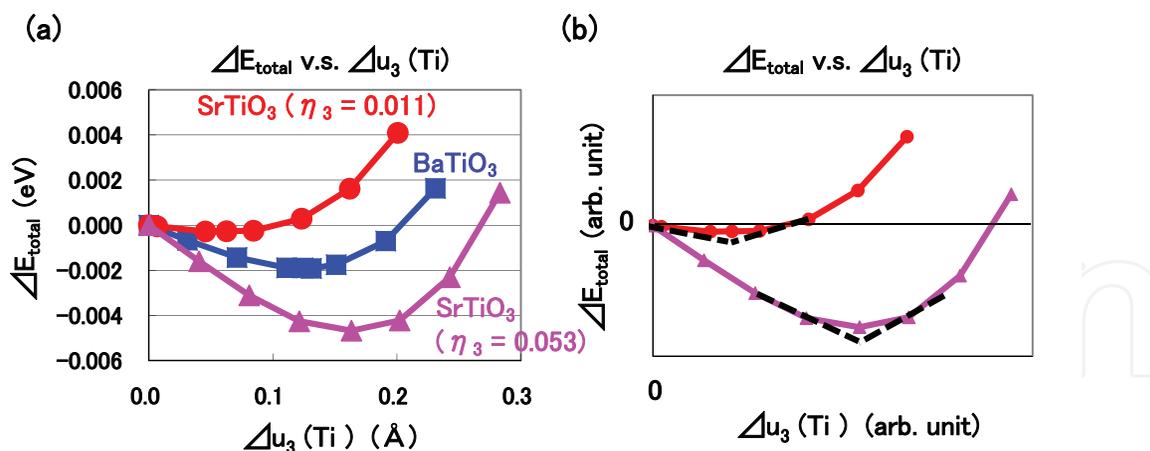
Fig. 13. (a) ΔE_{total} as a function of u_{Ti} in tetragonal SrTiO$_3$ and BaTiO$_3$. (b) Illustration of the ΔE_{total} curves in tetragonal SrTiO$_3$ ($\eta = 0.011$) and SrTiO$_3$ ($\eta = 0.053$) with deviations at the minimum point of ΔE_{total}.

absolute value of $Z^*_{Ti} \times \partial u_3(Ti)/\partial\eta_1$ (< 0) and $Z^*_{O_x} \times \partial u_3(O_x)/\partial\eta_1$ (> 0) in SrTiO$_3$ is larger than that in BaTiO$_3$. Figure 14(b) shows the difference between the A–O$_z$ distance (R_{A-O_z}) and $r_A + r_{O_z}$ on the (001) plane as a function of the ratio c/a. Note that R_{A-O_z} is smaller than $r_A + r_{O_z}$ in both SrTiO$_3$ and BaTiO$_3$. However, the difference in absolute value between R_{A-O_z} and $r_A + r_{O_z}$ in BaTiO$_3$ is larger than that in SrTiO$_3$. This result suggests that the Ba–O$_z$ Coulomb repulsion on the (001) plane in BaTiO$_3$ is larger than that in SrTiO$_3$ and that therefore O$_z$ ion of BaTiO$_3$ can be displaced along the [001] axis more easily than that of SrTiO$_3$, as discussed in previous subsection. This would be a reason why the absolute value of $\partial u_3(k)/\partial\eta_1$ of O$_z$ ion in BaTiO$_3$ is larger than that in SrTiO$_3$. Therefore, the absolute value of $Z^*_{O_z} \times \partial u_3(O_z)/\partial\eta_1$ (> 0) in BaTiO$_3$ is larger than that in SrTiO$_3$. Finally, as a result, the above investigations suggest that the signature of e_{31} in SrTiO$_3$ or BaTiO$_3$ is closely related to the difference in absolute values between $Z^*_{Ti} \times \partial u_3(Ti)/\partial\eta_1$ and the sum of $Z^*_{O_x} \times \partial u_3(O_x)/\partial\eta_1$ and $Z^*_{O_z} \times \partial u_3(O_z)/\partial\eta_1$.

4. Summary

Using a first-principles calculation with optimized structures, the author has investigated the role of the Coulomb repulsions between Ti 3s and 3p states and O 2s and 2p states in ferroelectric BaTiO$_3$. It has been found that the Coulomb repulsions between Ti 3s and $3p_{x(y)}$ states and O$_{x(y)}$ 2s and $2p_{x(y)}$ states are closely related to the appearance of Ti ion displacement in tetragonal BaTiO$_3$. This mechanism seems to be consistent with the appearance of Ti ion displacement in rhombohedral BaTiO$_3$. The present investigation suggests that the Coulomb repulsions between Ti 3s and 3p states and O 2p states have an important role in ferroelectricity. In addition to this suggestion, the author believes that the present investigation will show a guideline for the choice of PPs when first-principles calculations with PP methods are performed. The author has also investigated the ferroelectric and piezoelectric properties of SrTiO$_3$ and BaTiO$_3$ with in-plane compressive tetragonal structures using a first-principles calculation. It has been found that the ferroelectric structure even in SrTiO$_3$ appears with in-plane compressive structures. The piezoelectric constant e_{33} drastically increases in SrTiO$_3$ rather than that in BaTiO$_3$ as the tetragonal ratio c/a (> 1) is
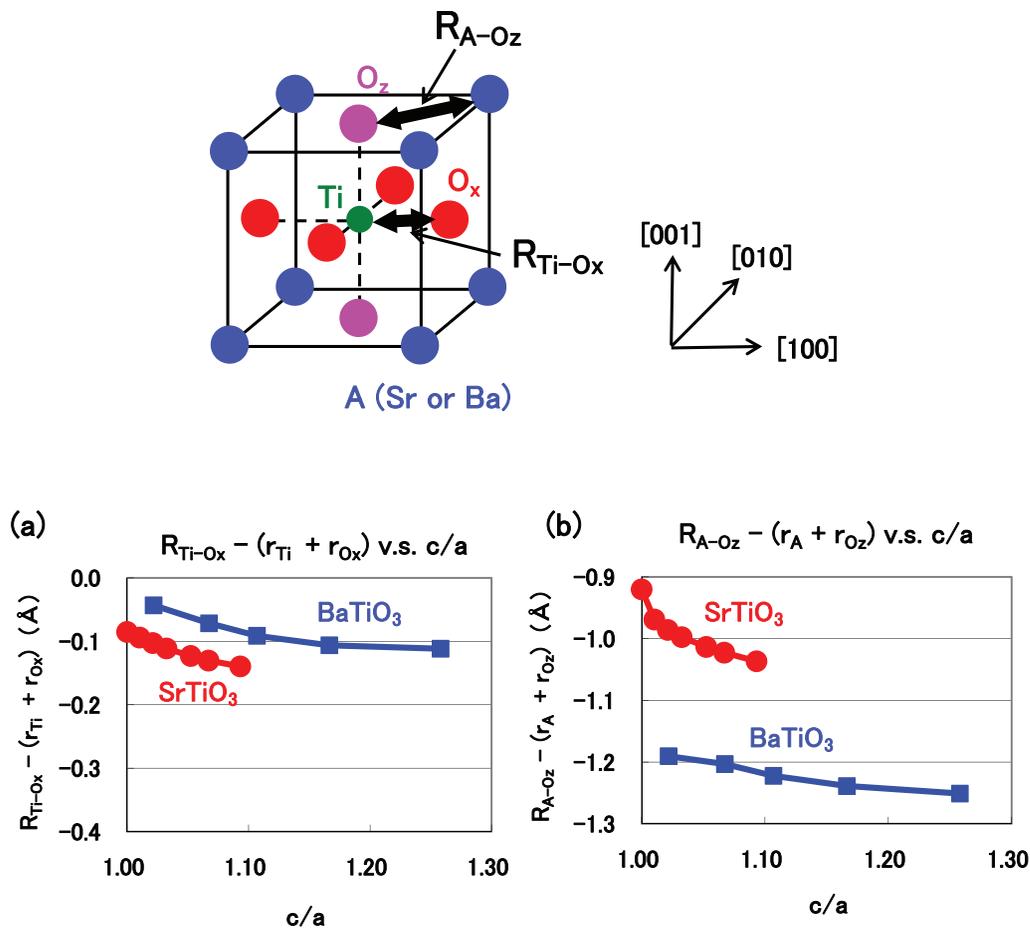
Fig. 14. Evaluated values as a function of c/a ratios in optimized tetragonal SrTiO$_3$ and BaTiO$_3$: (a) difference between the Ti–O$_x$ distance (R_{Ti-O_x}) and $r_{Ti} + r_{O_x}$, as a function of the ratio c/a, and (b) difference between the A–O$_z$ distance (R_{A-O_z}) and $r_A + r_{O_z}$. R_{Ti-O_x} and R_{A-O_z} in ATiO$_3$ are also illustrated (Furuta & Miura, 2010).

close to 1. On the other hand, e_{31} shows negative in SrTiO$_3$ while positive in BaTiO$_3$, although the changes in their absolute values are very small. The author has found that these properties of e_{33} and e_{31} in SrTiO$_3$ and BaTiO$_3$ are closely related to the ionic distances.

5. Acknowledgements

6. References

Ahart, M., Somayazulu, M., Cohen, R. E., Ganesh, P., Dera, P., Mao, H., Hemley, R., Ren, Y., Liermann, P. & Wu, Z. (2008). Origin of morphotropic phase boundaries in

ferroelectrics. *Nature*, Vol. 451, No. 7178, pp. 545-549.

Bévillon, É. & Geneste, G. (2007). Unstable polar mode and minimum of the dielectric constant in cubic BaSnO$_3$ under hydrostatic pressure. *Phys. Rev. B*, Vol. 75, No. 21, p. 214106 (5 pages).

Bousquet, E. & Ghosez, P. (2006). First-principles study of barium titanate under hydrostatic pressure. *Phys. Rev. B*, Vol. 74, No. 18, p. 180101(R) (4 pages).

Chen, X., Lu, W. & Shen, S. C. (2004). First-principles study of photoconductivity in BaTiO$_3$ with oxygen vacancies. *Solid State Commun.*, Vol. 130, No. 10, pp. 641-645.

Cohen, R. E & Krakauer, H. (1990). Lattice dynamics and origin of ferroelectricity in BaTiO$_3$: Linearized-augmented-plane-wave total-energy calculations. *Phys. Rev. B*, Vol. 42, No. 10, pp. 6416-6423.

Cohen, R. E. (1992). Origin of ferroelectricity in perovskite oxides. *Nature*, Vol. 358, No. 6382, pp. 136-138.

Damjanovic, D. (2010). A morphotropic phase boundary system based on polarization rotation and polarization extension. *Appl. Phys. Lett.*, Vol. 97, No. 6, p. 062906 (3 pages).

Diéguez, O., Rabe, K. M., & Vanderbilt, D. (2005). First-principles study of epitaxial strain in perovskites. *Phys. Rev. B*, Vol. 72, No. 14, p. 144101 (9 pages), and references therein.

Fujii, Y., Uwe, H. & Sakudo, T. (1987). Stress-Induced Quantum Ferroelectricity in SrTiO$_3$. *J. Phys. Soc. Jpn.*, Vol. 56, No. 6, pp. 1940-1942.

Furuta, T & Miura, K. (2010). First-principles study of ferroelectric and piezoelectric properties of tetragonal SrTiO$_3$ and BaTiO$_3$ with in-plane compressive structures. *Solid State Commun.*, Vol. 150, No. 47-48, pp. 2350-2353.

Gonze, X., Beuken, J.-M., Caracas, R., Detraux, F., Fuchs, M., Rignanese, G.-M., Sindic, L., Verstraete, M., Zerah, G., Jollet, F., Torrent, M., Roy, A., Mikami, M., Ghosez, Ph., Raty,J.-Y. & Allan, D. C. (2002). First-principles computation of material properties: the ABINIT software project. *Comput. Mater. Sci.*, Vol. 25, No. 3, pp. 478-492.

Gonze., X. et al. (2005). Informations on the Troullier-Martins pseudopotentials.
    URL: *http://www.abinit.org/downloads/psp-links/lda_tm_psp1_data*

Haeni, J. H., Irvin, P., Chang, W., Uecker, R., Reiche, P., Li, Y. L., Choudhury, S., Tian, W., Hawley, M. E., Craigo, B., Tagantsev, A. K., Pan, X. Q., Streiffer, K., Chen, L. Q., Kirchoefer, S. W., Levy, J. & Schlom, D. G. (2004). Room-temperature ferroelectricity in strained SrTiO$_3$. *Nature*, Vol. 430, No. 7001, pp. 758-761.

Hamann, D. R., Wu, X., Rabe, K. M. & Vanderbilt, D. (2005). Metric tensor formulation of strain in density-functional perturbation theory. *Phys. Rev. B*, Vol. 71, No. 3, p. 035117 (13 pages).

Khenata, R., Sahnoun, M., Baltache, H., Rérat, M., Rashek, A. H., Illes, N. & Bouhafs, B. (2005). First-principle calculations of structural, electronic and optical properties of BaTiO$_3$ and BaZrO$_3$ under hydrostatic pressure. *Solid State Commun.*, Vol. 136, No. 2, pp. 120-125.

Kornev, I. G., Bellaiche, L., Bouvier, P., Janolin, P.-E., Dkhil, B. & Kreisel, J. (2005). Ferroelectricity of Perovskites under Pressure. *Phys. Rev. Lett.*, Vol. 95, No. 19, p. 196804 (4 pages).

Kuroiwa, Y., Aoyagi, S., Sawada, A., Harada, J., Nishibori, E., Tanaka, M. & Sakata, M. (2001). Evidence for Pb-O Covalency in Tetragonal PbTiO$_3$. *Phys. Rev. Lett.*, Vol. 87, No. 21 p. 217601 (4 pages).

Miura, K. & Tanaka, M. (1998). Electronic structures of PbTiO$_3$: I. Covalent interaction between Ti and O ions. *Jpn. J. Appl. Phys.*, Vol. 37, No. 12A, pp. 6451-6459.

Miura, K. (2002). Electronic properties of ferroelectric $SrBi_2Ta_2O_9$, $SrBi_2Nb_2O_9$, and $PbBi_2Nb_2O_9$ with optimized structures. *Appl. Phys. Lett.*, Vol. 80, No. 16, pp. 2967-2969.

Miura, K., Kubota, M., Azuma, M. & Funakubo, H. (2009). Electronic and structural properties of $BiZn_{0.5}Ti_{0.5}O_3$ *Jpn. J. Appl. Phys.*, Vol. 48, No.9, p. 09KF05 (4 pages).

Miura, K., Furuta, T. & Funakubo, H. (2010a). Electronic and structural properties of $BaTiO_3$: A proposal about the role of Ti 3s and 3p states for ferroelectricity. *Solid State Commun.*, Vol. 150, No 3-4, pp. 205-208.

Miura, K., Kubota, M., Azuma, M. & Funakubo, H. (2010b). Electronic, structural, and piezoelectric properties of $BiFe_{1-x}Co_xO_3$. *Jpn. J. Appl. Phys.*, Vol. 49, No.9, p. 09ME07 (4 pages).

Miura, K. & Furuta, T. (2010). First-principles study of structural trend of BiMO$_3$ and BaMO$_3$: Relationship between tetragonal and rhombohedral structure and the tolerance factors. *Jpn. J. Appl. Phys.*, Vol. 49, No. 3, p. 031501 (6 pages), and references therein.

Miura, K., Azuma, M. & Funakubo, H. (2011). [Review] Electronic and structural properties of ABO$_3$: Role of the B–O Coulomb repulsions for ferroelectricity. *Materials*, Vol. 4, No 1, pp. 260-273.

Oguchi, T, Ishii, F. & Uratani, Y. (2009). New method for calculating physical properties from first principles–piezoelectric and multiferroics. *Butsuri*, Vol. 64, No. 4, pp. 270-276 (in Japanese).

Perdew, J. P. & Wang, Y. (1992). Accurate and simple analytic representation of the electron-gas correlation energy *Phys. Rev. B*, Vol. 45, No. 23, pp. 13244-13249.

Rappe, A. M. (2004). Opium–pseudopotential generation project.
    URL: *http://opium.sourceforge.net/index.html*

Resta, R. (1994). Macroscopic polarization in crystalline dielectrics: the geometric phase approach. *Rev. Mod. Phys.*, Vol. 66, No. 3, pp. 899-915.

Ricinschi, D., Kanashima, T. & Okuyama, M. (2006). First-principles study of tetragonality ratio and unit-cell volume influence on spontaneous polarization of $BaTiO_3$ and $PbTiO_3$. *J. Soc. Mater. Sci. Jpn.*, Vol. 55, No. 2, pp. 169-172 (in Japanese).

Shannon, R. D. (1976). Revised effective ionic radii and systematic studies of interatomic distances in halides and chalcogenides. *Acta Crystallogr., Sect. A*, Vol. 32, No. 5, pp. 751-767.

Uratani, Y., Shishidou, T. & Oguchi T. (2008). First-principles calculations of colossal piezoelectric response in thin film $PbTiO_3$. *Ext. Abst. Jpn. Soc. Appl. Phys.*, Vol. 55, No. 2, p. 566 (in Japanese).

Vanderbilt, D. (2000). Berry-phase theory of proper piezoelectric response. *J. Phys. Chem. Solids*, Vol. 61, No. 2, pp. 147-150, and references therein.

Wu X., Vanderbilt, D. & Hamann, D. R. (2005). Systematic treatment of displacements, strains, and electric fields in density-functional perturbation theory. *Phys. Rev. B*, Vol. 72, No. 3, p. 035105 (13 pages).

Wu, Z. & Cohen, R. E. (2005). Pressure-induced anomalous phase transitions and colossal enhancement of piezoelectricity in $PbTiO_3$. *Phys. Rev. Lett.*, Vol. 95, No. 3, p. 037601 (4 pages).
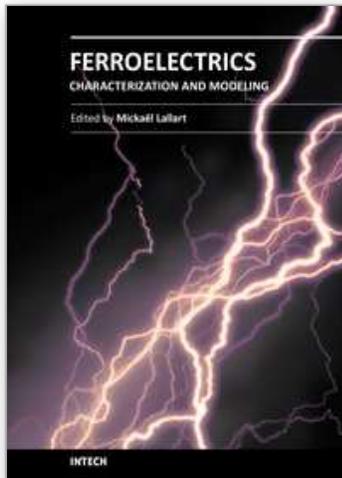
Ferroelectrics - Characterization and Modeling

Edited by Dr. Mickaël Lallart

Ferroelectric materials have been and still are widely used in many applications, that have moved from sonar towards breakthrough technologies such as memories or optical devices. This book is a part of a four volume collection (covering material aspects, physical effects, characterization and modeling, and applications) and focuses on the characterization of ferroelectric materials, including structural, electrical and multiphysic aspects, as well as innovative techniques for modeling and predicting the performance of these devices using phenomenological approaches and nonlinear methods. Hence, the aim of this book is to provide an up-to-date review of recent scientific findings and recent advances in the field of ferroelectric system characterization and modeling, allowing a deep understanding of ferroelectricity.

How to reference

In order to correctly reference this scholarly work, feel free to copy and paste the following:

Kaoru Miura (2011). First-Principles Study of ABO3: Role of the B–O Coulomb Repulsions for Ferroelectricity and Piezoelectricity, Ferroelectrics - Characterization and Modeling, Dr. Mickaël Lallart (Ed.), ISBN: 978-953-307-455-9, InTech, Available from: http://www.intechopen.com/books/ferroelectrics-characterization-and-modeling/first-principles-study-of-abo3-role-of-the-b-o-coulomb-repulsions-for-ferroelectricity-and-piezoelec

INTECH
open science | open minds